ADVANCED SUSTAINABLE SYSTEMS
www.advsustainsys.com

Electrochemical Hydrogen Storage in Amine-Activated Polydopamine

*Halime Coskun, Abdalaziz Aljabour, Theresia Greunz, Matthias Kehrer, David Stifter, and Philipp Stadler**

Electrochemical hydrogen storage combines the evolution, oxidation, and storage of hydrides from aqueous electrolytes and ionic liquids, but presently requires palladium or rare-earth metals to achieve significant power capacities. Here hydrogen electrosorption in amine-activated polydopamine is shown. The organic heterogeneous amine-hydride yields a gravimetric hydrogen density of 0.44%, corresponding to a 80% hydride-per-monomer content, and offers similar reaction kinetics as for palladium and related systems. An initial stability test of 100 electrosorption cycles that demonstrates resilience in acidic media with a tendency for increased capacity over time is included. In situ vibronic amine-hydride fingerprints corroborate the reversibility and stability of the conversion process and highlight the merits of amine-activated polydopamines as a heterogeneous organic hydrogen storage system.

1. Introduction

Safe and low-cost methods for reversible proton-hydrogen conversion are the driving force for powering electric devices based on carbon-neutral energy cycles.[1–5] Electrochemical hydrogen storage consolidates proton-reduction, hydride storage and hyride re-oxidation offering a variety of applications such as rechargeable batteries or electrochemical capacitors.[6–8] However, only few catalytic metals and metal composites, among them palladium and rare-earth metals alloys, show hydrogen electrosorption (HES). Hydrogen is thereby chemisorbed as interstitial hydride of type MeH_x.[9–18] HES is reversible, nonetheless, limited by unwanted side-reactions such as metal oxidation and lattice expansion. These reduce the storage capacity over time.[19] Recent developments used multicomponent metal alloys to reduce overoxidation and lattice deformations.[18,20–26] In additon, cost-reduction was demonstrated by implementing carbon materials.[1,27–39] Recently enhanced stability and reversiblity was shown by Pajak et al. by demonstrating hydrogen electrosorption electrosorption from ionic liquids.[40,41] However, electrochemical hydrogen storage requires still the vast usage of critical and eventually toxic metals.[9,42,43]

In this work, we present a heterogeneous organic amine-hydride system as metal-free alternative. We sought to activate amines in conducting polydopamine for HES to achieve a stable and reversible electrochemical hydride system operating in aqueous media at ambient pressures and temperatures. Earlier works revealed the nature of amines in polydopamines steer the selectivity; indole (and indoline) favored electrocatalytic hydrogen-evolution, while primary amines, such as the dopamine $(\text{-DA-})_n$ building block, possessed large binding energies for as-reduced hydrogen.[46] From that we hypothesized that (primary) amine-activation in polydopamine led to hydrogen electrosorption.

We subsequently modified the structure of polydopamine toward mainly $(\text{-DA-})_n$ monomers and by that achieved a polymer with mainly primary amines ($-NH_2$) based on prior art synthesis.[44–46,48,49] We reduced the reaction temperature of the oxidative chemical vapor deposition (oCVD) polymerization to 150 °C and achieved a polymer with 70% primary amines. This amine-activated polydopamine (aaPDA) showed effective HES similar to palladium with a maximum of the hydrogen capacity close to –0.2 V versus RHE. At higher cathodic potentials, the hydride formation was gradually superseded by hydrogen evolution. We found HES was reversible: The re-oxidation peak occurred at +0.5 V, so that the potential difference between absorption and desorption spanned 0.6 V. This difference was substantially higher as compared to metal-hydrides aiding the system's resilience against overoxidation. aaPDA achieved a gravimetric hydrogen density equal to PdH_x at 0.44%. This corresponded to 80% of the monomers activated for HES leading to a coulometric capacity of 0.12 Ah g^{-1}. We included an initial stability test with 100 electrosorption cycles and report the continuous activation of aaPDA over time.

Dr. H. Coskun, Dr. A. Aljabour, Dr. P. Stadler
Institute of Physical Chemistry
Johannes Kepler University Linz
Altenberger Strasse 69, Linz 4040, Austria
E-mail: philipp.stadler@jku.at
Dr. T. Greunz, M. Kehrer, Prof. D. Stifter
Center for Surface and Nanoanalytics
Johannes Kepler University Linz
Altenbergerstrasse 69, Linz 4040, Austria
Dr. P. Stadler
Linz Institute of Technology (LIT)
Johannes Kepler University Linz
Altenbergerstr. 69, Linz A-4040, Austria
The ORCID identification number(s) for the author(s) of this article can be found under https://doi.org/10.1002/adsu.202000176.

DOI: 10.1002/adsu.202000176

These results were supported by in situ vibration spectroelectrochemistry revealing signature features of rising NH-vibrations upon electrochemical reduction. We concluded with discussing heterogeneous amine-hydrogen storage as important step toward using hydrogen as energy carrier without requiring the evolution of molecular H_2.

2. Results and Discussion

Amines in conducting polydopamine were shown to steer electrocatalytic selectivity in different directions (**Figure 1**): Secondary amines, such as in the condensed indoline and indole-fragments, implement hydrogen evolution reaction (HER).[46–48] Primary amines, such as present in the dopamine $(\text{-DA-})_n$ building block, possessed too high binding energies so that they suppress the hydrogen evolution but therefore enable hydrogen electrosorption (HES).

We found it attractive to harness electrocatalytic amines in dopamine for a heterogeneous amine-hydride with the aim to substitute classic PdH_x and related metal composite systems. For this, we synthesized amine-activated polydopamine (aaPDA) based on earlier experiments (Figure 1a): We referred to oxidative chemical vapor deposition (oCVD) polymerization using dopamine as educt monomer.[45] We modified the oCVD in the sense to reduce the temperature in the reaction zone to maximum 150 °C to balance the oxidation power and to favor the direct oxidative polymerization (and doping) of dopamine, whilst suppressing its unwanted oxidation to i) dopaminequinone or ii) leucodopaminechrome and 5,6-dihydroxyindole. Such quenching of the reaction temperatures to 150 °C, more than 50% compared to the vaporization temperature at 320 °C, led to dopamine $(\text{-DA-})_n$ as the main building block to result as aaPDA (Figure 1a): we achieved an average ratio of 7:3 between primary amines (NH_2 from dopamine and dopaminequinone) and secondary amines (–NH- from indoline and indole derivatives) indicated by the high resolution scan of the N1s XPS pattern (Figure 1b). We also resolved the O1s pattern with a ratio of 2.6:1 between hydroxy- to quinone that similarly pointed at a suppressed quinoid formation (Figure 1c). Further, the O1s patterns indicated a maintained doping ratio (monomer:bisulfate), here reported at 3.2:1 (i.e., more than every third monomer doped); the latter corresponded to conducting polydopamines and other related conducting polymers.[49–51]

Based on the presence of 70% primary amines, the aaPDA possessed electrosoprtion-selective hydrogen-bonds from primary amines in combination with adjacent hydroxy- and keto-groups, along the entire electrically conducting backbone. These functions acted as the hydride formation centers with a theoretical maximum capacity of one proton per monomer (Figure 1d). To study HES, we deposited the aaPDA directly on carbon, which served as inert carrier electrode. The electrochemical characterization included cyclic voltammogram and chronoamperometric/chronocoulometric scans as well as spectroelectrochemical in situ ATR-FTIR (electrochemical-induced absorption, EIA). We consistently used 1 M trifluoromethanesulfonic acid (TfOH, pH = 0) as the electrolyte at 25 °C and 1 atm. This specific electrolyte acted as inert proton source. We referred all electrochemical data versus the reversible hydrogen electrode (RHE, pH = 0). Fingerprint feature of HES in the cyclic voltammogram was the steep rise of the electric Faraday current starting at an electrochemical underpotential versus RHE. The steep rise peaked at –0.2 V versus RHE, where quantitative amounts of hydrogen were electrosorbed (**Figure 2**a). By sweeping further to the negative, the current decreased to a local minimum at –0.4 V versus RHE. Beyond this potential, the current rose again and hydrogen evolution was observed (steep exponential rise of the current). In the reverse scan, the voltammogram showed a flattened profile coinciding to an isosbestic point at +0.2 V versus RHE. At +0.51 V, we observed the maximum of the re-oxidation peak of the electrosorbed hydride to the proton. The forward-scan showed also an isosbestic point at an similar potential around +0.2 V.

The cyclic voltammograms (CVs, 100 consecutive scans) exhibited reversible electrosorption including ab- and desorption peaks with a potential difference of average 0.6 V (Figure 2a). The peak currents increased gradually by repeating number of cycles, which we assigned to a change of the local pH in the vicinity of the electrode paired with a continuous slight activation of aaPDA. The presence of isobestic points in forward and back-scans (+0.2 V vs RHE) provided evidence that the electrosorption progressed without notable side reactions. These results demonstrated the reversibility of the aaPDA as electrosorptive electrode. The potential difference aided the resilience of amine-hydrides as compared to metals (with characteristic only 0.15 V).[15] In addition, we used chronocoulometry to show the dynamics of electron and proton transfer measured at the maxima of absorption and desorption (–0.2 V and +0.51 V vs RHE, respectively, Figure 2b). For absorption two characteristic regimes were observed: a fast capacitive and slower diffusion-controlled regime with different reaction constants. For desorption, we subtracted the capacitive baseline currents as these were substantial. From chronocoulometry we derived the reaction rates $k_{red/ox}$ for reduction 0.034 and re-oxidation 0.018 s^{-1} corresponding to 30–50 s (linear fit in Figure S1, Supporting Information). According to that, we found a gravimetric hydrogen storage capability close to 80% electrosorbed hydrogen per monomer within 30–50 s ($k_{red/ox}^{-1}$). This corresponded to a power capacity of 0.120 Ah g^{-1} or a gravimetric hydrogen density ω_H of 0.44% (Equations (1) and (2)). The theoretic limit for hydrogen storage in aaPDA corresponds to 1 proton per monomer (1 amine in $(\text{-DA-})_n$, ω_H equals 0.56%).

$$\omega_H = \frac{0.8 \times M_{\text{H}}}{M_{\text{aaPDA}}} \tag{1}$$

$$M_{\text{aaPDA}} = M_{(-\text{DA}-)} + \frac{M_{\text{HSO}_4^-}}{3.2} = 181.5 \text{ g mol}^{-1} \tag{2}$$

The factor 3.2 accounted to the ratio between the monomer (-DA-) and bisulfate (HSO_4^-) as derived from the XPS-scans (3.2:1 corresponds to the frequently observed Coulomb limit of conducting polymers, Figure 1c).[51]

Further chronoamperometric scans were recorded at different electrosorption potentials that revealed a similar charge (and proton) dynamics: We varied the potentials close to RHE = 0 (absorption) (**Figure 3**a) and at the desorption peak around +0.5 V versus RHE, respectively (Figure 3b). These

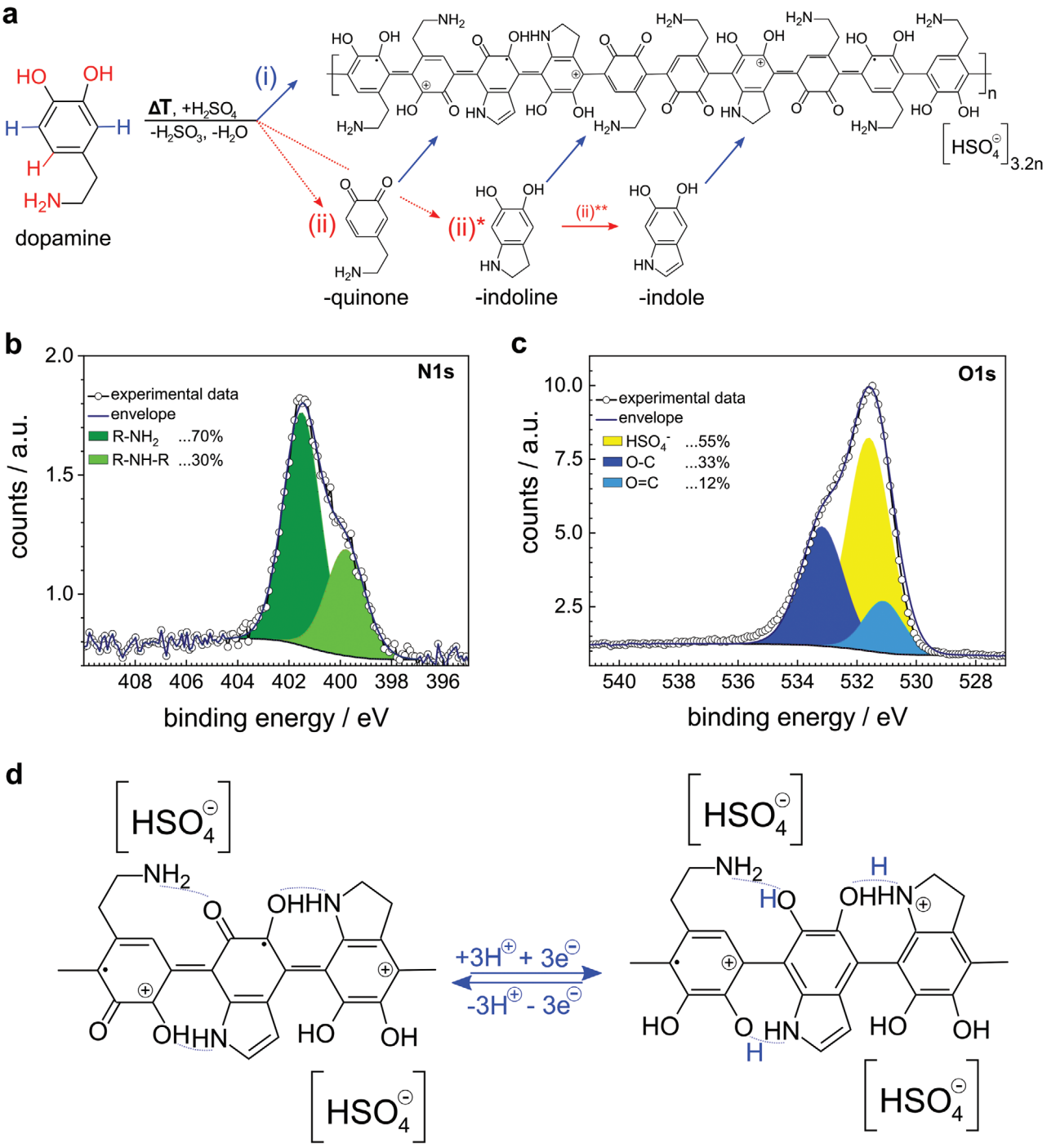

Figure 1. Structure of oxidative CVD-synthesized amine-activated polydopamine: a) 150 °C synthesis path favoring i) direct polymerization and suppressing, ii) intermediate side-oxidation to the corresponding quinone or indoline (and indol) to result amine-activated polydopamine (aaPDA). b) N1s XPS high-resolution XPS revealed the ratio is 7:3 between primary (dopamine) amines and secondary (indoline and indole) amines. c) O1s high-resolution XPS revealed 55% of oxygen from bisulfate yielding a monomer:sulfate ratio of 3.2:1 (doping concentration). Further it showed a 3:1 ratio between dopamine:quinone, i.e. 38% of hydroxy-groups reacted to the corresponding quinoid form. d) Electrosorption reaction mechanism: amine-activated aaPDA can take up to one proton per monomer. The mechanism suggested the formation of an additional N–H bond.

results corroborate the characteristic 2-regime dynamics earlier reported in PdH_x with capacitive and diffusion-controlled regimes indicated by the steep decay and subsequent saturation or slight decrease of the current.[15] From that, we derived the potentiocoulometry for the initial electrosorption regime (integrated first 10 s) that shows the immediate charging occurring to up to 80% capacity protons per monomer, $(\text{-DA-})_n$) (Figure 3c,d). In these scans we considered the upper and lower

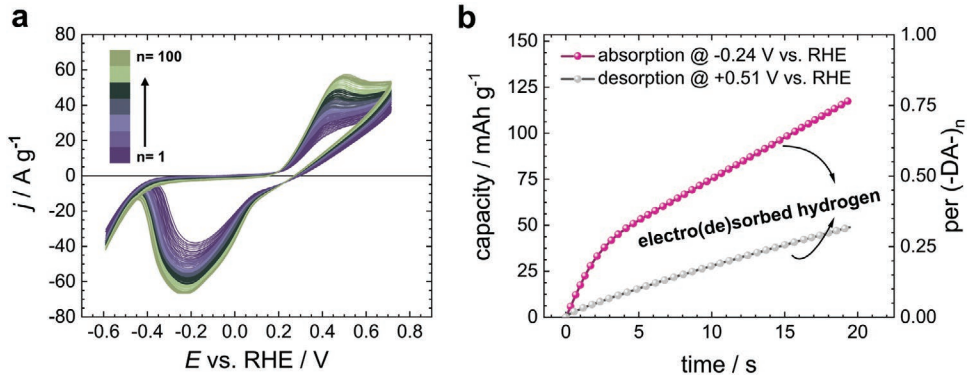

Figure 2. Cyclic voltammogram and charge balance: a) Gravimetric current density j showed reversible hydrogen electrosorption (HES) with negative reduction peak at –0.24 V, positive re-oxidation peak at +0.54 V and the isobestic point minima at +0.2 V. The cyclic voltammogram (50 mV s^{-1}) revealed a rising electrosorption current with repeating number of cycles. b) Chronocoulometric scans at the reduction and re-oxidation peak maxima indicated the proton-to-hydride reaction constants reaching 0.8 protons per monomer after 20 s.

potential limits, for reduction higher than –0.34 V versus RHE (hydrogen evolution) and for re-oxidation beyond +0.8 V versus RHE (oxidation of polymer). For qualitative analysis of the intermediately formed amine-hydrides we used electrochemical-induced absorption spectroscopy (EIA) in the infrared. The study probed vibronic changes during proton reduction/re-oxidation. We therefore installed a 2-electrode configuration without liquid electrolyte, in order to reduce the spectral background noise (Figure S2, Supporting Information): we applied a (solution-processed) proton membrane between aaPDA and an inert platinum counter electrode. aaPDA was deposited on germanium (**Figure 4**a) serving as carrier electrode and ATR element. With that, we studied HES by linear sweep voltammetry and in situ ATR-FTIR. The reference potentials were determined by the current-voltage scans using reduction- and re-oxidation peaks as well as the local minima at the isosbestic points (+0.2 V vs RHE, Figure 4a, inset). From that we scanned multiple spectra (T_{min}, T_{max}) at +0.2 V versus RHE (current minima) and at –0.2 V versus RHE (maximum of absorption) and referenced them against the baseline reference scan

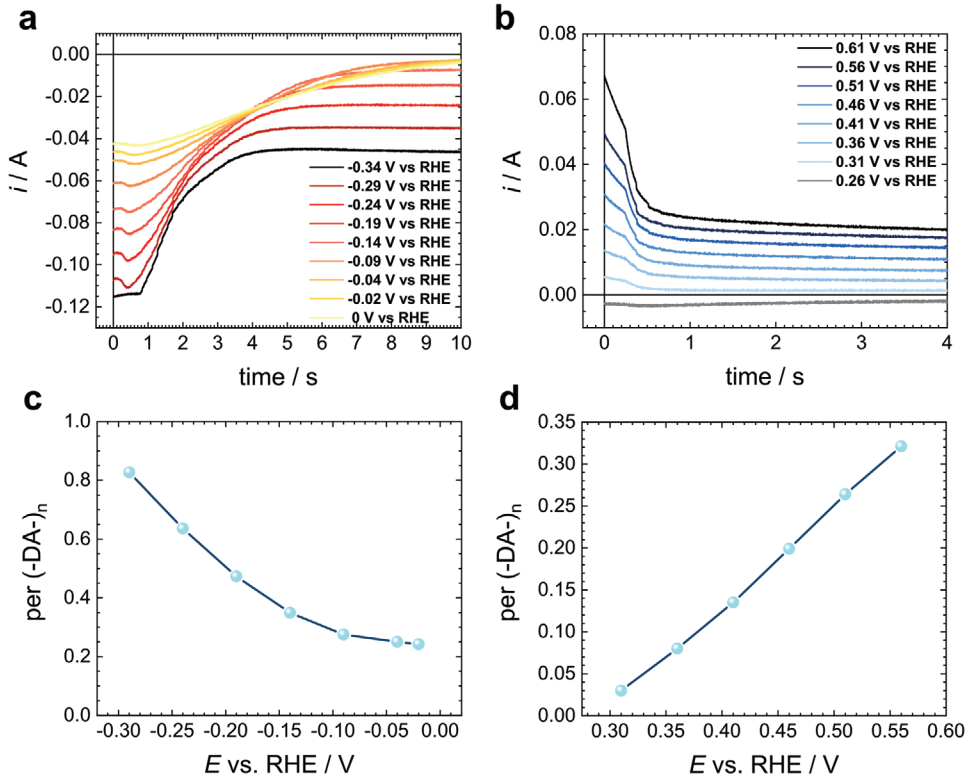

Figure 3. Electrodynamics of HES: a) Chronoamperometry shows the absorption of protons in aaPDA at increasing potentials from 0 to –0.34 V versus RHE. b) Corresponding decharging chronoamperometry at potentials from +0.26 to +0.61 V versus RHE. c) Integrated charge per dopamine monomer, $(\text{-DA-})_n$ for the absorption and d) desorption process.

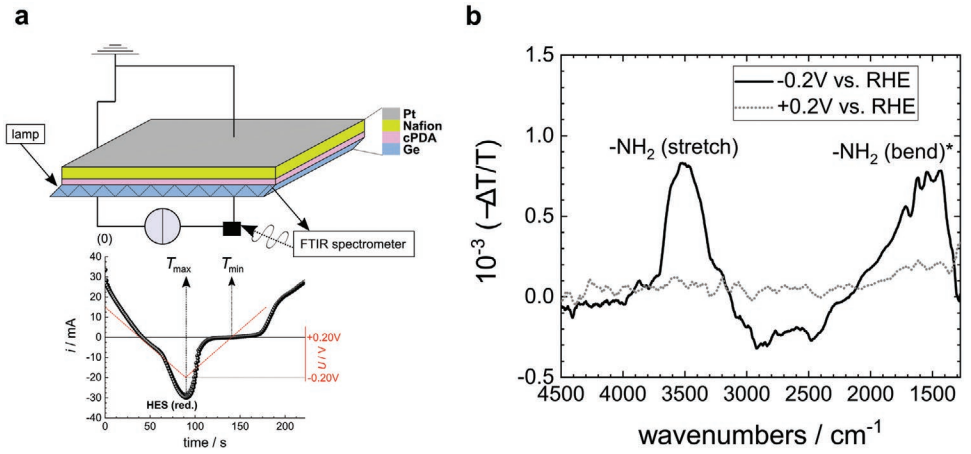

Figure 4. Electrochemical-induced absorption: a) ATR-FTIR schematic for measuring spectral changes while HES in aaPDA. We determine particular the (operando)absorption spectra at the maximum and minimum (T_{max} and T_{min}) of electrosorption against the spectra without bias (T_0, T = transmission). (b) Differential spectra at the maximum and minimum of electrosorption reveals the changes: baseline (T_{min}) and amine features (T_{max}) arising because of electrosorbed hydrogen in aaPDA.

without bias (T_0). The differential absorption spectra ($-\Delta T/T \approx$ absorption, T is transmission) showed the vibronic changes induced by electrosorption: while at +0.2 V versus RHE (T_{min}) we observed practically no changes, at −0.2 V versus RHE (T_{max}) we report emerging fingerprint features corresponding to NH_2 stretch vibrations (maximum at 3500 cm^{-1}) and the NH_2 bend vibrations (1550 to 1650 cm^{-1}); the signals are broadened by hydrogen-bonds with adjacent hydroxide stretch and bending vibrations (Figure 4a).

Technological solutions for electrochemical hydrogen storage are decisive to increase the implementation of hydrogen as energy carrier. Presently, reversible electrosorbed hydrides are formed only on special noble or rare-earth metals and metal-composites. The here presented electrocatalytic organic hydride, inspired by the ammonia-hydrogen storage system, created a solution without demanding metals. Central were thereby the activated (primary) amines in polydopamine that enabled reversible hydrogen electrosorption. We showcased that the process was revocable and offered equal reaction kinetics and storage capacities as metal-hydrides. Furthermore, we found the electrocatalytic activity increased over time pointing at controlled ab- and desorption kinetics progressing without significant side-reactions. We corroborated these results by in situ vibration spectroelectrochemistry: the fingerprint spectra showed the emergence of the proposed hydrided bonds upon electrochemical bias. We conclude with pointing at the applicability of the amine-activated polydopamines for electrochemical hydrogen storage, and, further, the importance of such system for rechargeable (aqueous-based) batteries and electrochemical capacitors.

3. Experimental Section

Synthesis and Characterization: Amine-activated polydopamine (aaPDA) was synthesized by oxidative chemical vapor deposition (oCVD) from dopamine hydrochloride and sulfuric acid according to Coskun et al.[45] with a modified reactor: A long quenching path of 20 cm was inserted between vaporization-zone (dopamine and sulfuric acid, 320 °C) and reaction (and deposition) zone, which remained unheated. By that the temperature in the reaction zone (close to the substrate) was leveled to a maximum 150 °C.

aaPDA was deposited on carbon felt (CF) (10 mm × 10 mm) (SGL Group, The Carbon Company, SEM before and after electrosoprtion in Figure S10, Supporting Information) and, for spectroelectrochemistry, on germanium. Prior deposition of the active layer, all substrates are cleaned using ultrasonic bath 15 min each in acetone, isopropyl alcohol, Hellmanex-detergent (Hellma, 70 °C) and deionized water. Before starting the synthesis, dopamine hydrochloride (Sigma-Aldrich) was dried in the oven at 150 °C overnight in presence of CaH_2 (95%, Sigma-Aldrich) to remove any water residual. The reaction was carried out in a tube furnace (Carbolite company; glass tube length: 45 cm; tube diameter: 2.4 cm) at a vaporization temperature of 320 °C under nitrogen atmosphere with a carrier gas-flow of 3 L min^{-1}. Sulfuric acid (95–97%, J.T. Baker) and sodium sulfate (≥99.0%, Sigma-Aldrich) are used as oxidation agent and corresponding salt, to enhance the balance toward SO_3^- and SO_4^{2-} in the gas phase. The chemical composition of aaPDA was determined by X-ray photoelectron spectroscopy (XPS). All measurements were recorded on aaPDA directly deposited on carbon felt electrodes. A Theta Probe from ThermoFisher Scientific was applied with an Al K_α (1486.7 eV) source. The charge was compensated by a Dual Flood Gun (1-2 eV electrons and Ar^+ ions), and the lens mode was set to standard. The energy pass amounted to 200 eV for the survey scan and to 50 eV for high-resolution (HR) scans, with energy steps of 1 and 0.1 eV, respectively. For data analysis, the Avantage v5.32 software package was used. The data fittings were in agreement with results described in the literature. The elemental concentrations were determined by survey and HR scans shown in Figure 1b,c (N1s and O1s) as well as in Supporting Information (spectral survey scan, C1s, S2p, Figures S4– S6 and N1s, S2p and F1s as-deposited, before and after hydrogen electrosorption, Figures S8– S9, Supporting Information).

Electrochemical Characterization: Electrochemical experiments were carried out using a JAISSLE Potentiostat Galvanostat IMP 88 PC. To examine amine-activated polydopamine (aaPDA) in HES, electrochemical studies were conducted in a standard three-electrode arrangement in an H-cell configuration (separated cathode space). A PDA-coated carbon felt (CF) was used as a working electrode (WE), Pt as a counter electrode (CE), and Ag/AgCl (3 M KCl) as a reference electrode (RE, +0.197 V vs the standard hydrogen electrode, SHE). All experiments (except those related to spectroelectrochemistry) were carried out in a 1 M trifluoromethanesulfonic acid (TfOH, pH = 0) as the electrolyte solution at 25 °C. The compartments were connected by a bridge using glass frit (porosity No. 2). All results reported were calculated versus the reversible hydrogen electrode (vs RHE equal to SHE at pH = 0) at scan rates of 50 and 5 mV s^{-1} (Figure S12, Supporting Information). For comparison, a CV

was included in 1 M HCl as alternative electrolyte (Figure S11, Supporting Information). The cell constants were characterized by electrochemical impedance spectroscopy (EIS) using an IVIUM compactstat (The Netherlands). At the open circuit potential (OCP) the impedance spectra were recorded in the range from 10^{-1} to 10^{5} Hz with a perturbation amplitude of 50 mV in standard electrode configurations (Pt-Pt, Pt-CF, Pt-CF-aaPDA, Figure S3 and Table S1, Supporting Information).

Spectroelectrochemistry: Electrochemical-induced absorption (EIA) was recorded in situ using internal reflection mode attenuated total reflection (ATR) - FTIR. The measurements were performed on a Bruker IFS 66/S Spectrometer. The in situ specimen consists of a germanium ATR element (parallelepiped, 1 × 10.5 mm, 45°, Harrick Scientific Products Inc.), which co-served as working electrode carrier. On top aaPDA (working electrode, WE) and a Pt counterelectrode (CE) resembling a 2-electrode electrochemical cell (Figure 4a) were deposited. As electrolyte, an activated proton membrane was used (Nafion 117, Sigma-Aldrich, SEM picture in Figure S7, Supporting Information), which was deposited by drop casting from solution onto aaPDA/germanium. EIA was recorded by recording reference spectra (without bias, T_0) and biased spectra at two potentials: one at the maximum of the electrosorption peak (corresponding to –0.2 V vs RHE, T_{max}) and one at the onset of electrosorption (corresponding to +0.2 V vs RHE, T_{min}). The potentials were referenced to the isosbestic point at +0.2 V versus RHE (minimum of current) from the curren–voltage scans of the 2-electrode cell (inset in Figure 4a). To improve the signal-to-noise, the measurements were repeated 100 times (noise level shown in Figure S2, Supporting Information). EIA spectra were then calculated by subtracting (and normalizing) the accumulated reference and bias scans according to Equation (3).

$$-\frac{\Delta T}{T} = -\frac{T_{min/max} - T_0}{T_0} \simeq -ln(T) = A \tag{3}$$

The spectra ($-\Delta T/T$) showed the differential absorption induced by electrochemcial bias. The positive spectral vibration features correspond to bonds formed by electrosorption.

Supporting Information

Supporting Information is available from the Wiley Online Library or from the author.

Acknowledgements

The authors acknowledge the financial support of the Austrian Science Foundation (FWF I3822-N37, Sustainable Catalysis), the Linz Institute of Technology (LIT, LIT-2017-4-YOU-005, Biopolymer-based carbonate reduction) at the Johannes Kepler University Linz, the European Regional Development Fund (EFRE, IWB2014-2020, 2018-98299 Articial Food and project BIOCARB-K), and the Government of Upper Austria.

Conflict of Interest

The authors declare no conflict of interest.

Keywords

amine-hydride, conducting polymers, electrochemical hydrogen storage, hydrogen electrosorption, polydopamine

Received: July 29, 2020
Revised: September 3, 2020
Published online:

[1] A. Dillon, M. Heben, *Appl. Phys. A: Mater. Sci. Process.* **2001**, *72*, 133.
[2] P. Preuster, C. Papp, P. Wasserscheid, *Acc. Chem. Res.* **2017**, *50*, 74.
[3] G. Crabtree, M. Dresselhaus, *MRS Bull.* **2008**, *33*, 421.
[4] A. Zuttel, A. Remhof, A. Borgschulte, O. Friedrichs, *Philos. Trans. R. Soc., A* **2010**, *368*, 3329.
[5] A. Schoedel, Z. Ji, O. M. Yaghi, *Nat. Energy* **2016**, *1*, 16034.
[6] J. Kleperis, G. Wójcik, A. Czerwinski, J. Skowronski, M. Kopczyk, M. Beltowska-Brzezinska, *J. Solid State Electrochem.* **2001**, *5*, 229.
[7] M. Baldauf, D. Kolb, *Electrochim. Acta* **1993**, *38*, 2145.
[8] B. Conway, B. Tilak, *Electrochim. Acta* **2002**, *47*, 3571.
[9] G. Jerkiewicz, *Prog. Surf. Sci.* **1998**, *57*, 137.
[10] M. Grdeń, A. Czerwiński, J. Golimowski, E. Bulska, B. Krasnodębska-Ostręga, R. Marassi, S. Zamponi, *J. Electroanal. Chem.* **1999**, *460*, 30.
[11] M. Grdeń, A. Piaścik, Z. Koczorowski, A. Czerwiński, *J. Electroanal. Chem.* **2002**, *532*, 35.
[12] M. Łukaszewski, K. Kuśmierczyk, J. Kotowski, H. Siwek, A. Czerwiński, *J. Solid State Electrochem.* **2003**, *7*, 69.
[13] M. Łukaszewski, M. Grdeń, A. Czerwiński, *J. Electroanal. Chem.* **2004**, *573*, 87.
[14] M. Łukaszewski, A. Żurowski, M. Grdeń, A. Czerwiński, *Electrochem. Commun.* **2007**, *9*, 671.
[15] M. Łukaszewski, A. Żurowski, A. Czerwiński, *J. Power Sources* **2008**, *185*, 1598.
[16] M. Łukaszewski, K. Klimek, A. Żurowski, T. Kędra, A. Czerwiński, *Solid State Ionics* **2011**, *190*, 18.
[17] L. Gai, Y. K. Shin, M. Raju, A. C. T. van Duin, S. Raman, *J. Phys. Chem. C* **2016**, *120*, 9780.
[18] G. Li, H. Kobayashi, J. M. Taylor, R. Ikeda, Y. Kubota, K. Kato, M. Takata, T. Yamamoto, S. Toh, S. Matsumura, H. Kitagawa, *Nat. Mater.* **2014**, *13*, 802.
[19] Y. Sakamoto, K. Yuwasa, K. Hirayama, *J. Less Common Met.* **1982**, *88*, 115.
[20] K. Hubkowska, A. Czerwiński, *J. Solid State Electrochem.* **2020**, https://doi.org/10.1007/s10008-020-04776-y.
[21] B. D. Adams, C. K. Ostrom, A. Chen, *Langmuir* **2010**, *26*, 7632.
[22] U. Koss, M. Łukaszewski, K. Hubkowska, A. Czerwiński, *J. Solid State Electrochem.* **2011**, *15*, 2477.
[23] A. Żurowski, M. Łukaszewski, A. Czerwiński, *Electrochim. Acta* **2006**, *51*, 3112.
[24] L. Roué, D. Guay, R. Schulz, *J. Electroanal. Chem.* **2000**, *480*, 64.
[25] M. Jafarian, O. Azizi, F. Gobal, M. Mahjani, *J. Alloys Compd.* **2007**, *432*, 74.
[26] C. Cachet-Vivier, S. Bastide, C. Zlotea, Y. Oumellal, M. Laurent, M. Latroche, *Electrochim. Acta* **2017**, *228*, 528.
[27] R. Ströbel, L. Jörissen, T. Schliermann, V. Trapp, W. Schütz, K. Bohmhammel, G. Wolf, J. Garche, *J. Power Sources* **1999**, *84*, 221.
[28] K. Jurewicz, E. Frackowiak, F. Béguin, *Appl. Phys. A* **2004**, *78*, 981.
[29] C. Vix-Guterl, E. Frackowiak, K. Jurewicz, M. Friebe, J. Parmentier, F. Béguin, *Carbon* **2005**, *43*, 1293.
[30] E. Yoo, L. Gao, T. Komatsu, N. Yagai, K. Arai, T. Yamazaki, K. Matsuishi, T. Matsumoto, J. Nakamura, *J. Phys. Chem. B* **2004**, *108*, 18903.
[31] E. Yoo, T. Habe, J. Nakamura, *Sci. Technol. Adv. Mater.* **2005**, *6*, 615.
[32] F. Béguin, M. Friebe, K. Jurewicz, C. Vix-Guterl, J. Dentzer, E. Frackowiak, *Carbon* **2006**, *44*, 2392.
[33] F. Béguin, K. Kierzek, M. Friebe, A. Jankowska, J. Machnikowski, K. Jurewicz, E. Frackowiak, *Electrochim. Acta* **2006**, *51*, 2161.
[34] J. Skowroński, A. Czerwiński, T. Rozmanowski, Z. Rogulski, P. Krawczyk, *Electrochim. Acta* **2007**, *52*, 5677.
[35] D. Qu, *J. Power Sources* **2008**, *179*, 310.
[36] M. Bleda-Martínez, J. Pérez, A. Linares-Solano, E. Morallón, D. Cazorla-Amorós, *Carbon* **2008**, *46*, 1053.
[37] B. Fang, M. Kim, J. H. Kim, J.-S. Yu, *Langmuir* **2008**, *24*, 12068.
[38] G. Lota, K. Fic, K. Jurewicz, E. Frackowiak, *Open Chem.* **2011**, *9*, 20.

[39] K. Babeł, K. Jurewicz, *Carbon* **2008**, *46*, 1948.
[40] M. Pająk, K. Hubkowska, A. Czerwiński, *Electrochim. Acta* **2019**, *324*, 134851.
[41] M. Pajaąk, K. Hubkowska, A. Czerwiński, *Electrochem. Commun.* **2020**, *118*, 106805.
[42] A. Czerwiński, R. Marassi, S. Zamponi, *J. Electroanal. Chem. Interfacial Electrochem.* **1991**, *316*, 211.
[43] B. D. Adams, A. Chen, *Mater. Today* **2011**, *14*, 282.
[44] H. Coskun, A. Aljabour, P. De Luna, D. Farka, T. Greunz, D. Stifter, M. Kus, X. Zheng, M. Liu, A. W. Hassel, W. Schöfberger, E. H. Sargent, N. S. Sariciftci, P. Stadler, *Sci. Adv.* **2017**, *3*, e1700686.
[45] H. Coskun, A. Aljabour, L. Uiberlacker, M. Strobel, S. Hild, C. Cobet, D. Farka, P. Stadler, N. S. Sariciftci, *Thin Solid Films* **2018**, *645*, 320.
[46] H. Coskun, A. Aljabour, P. D. Luna, H. Sun, N. Nishiumi, T. Yoshida, G. Koller, M. G. Ramsey, T. Greunz, D. Stifter, A. W. Hassel, N. S. Sariciftci, E. H. Sargent, P. Stadler, *Adv. Mater.* **2020**, https://doi.org/10.1002/adma.201902177.
[47] Y. Zheng, Y. Jiao, Y. Zhu, L. H. Li, Y. Han, Y. Chen, A. Du, M. Jaroniec, S. Z. Qiao, *Nat. Commun.* **2014**, *5*, 3783.
[48] H. Coskun, A. Aljabour, W. Schöfberger, A. Hinterreiter, D. Stifter, N. S. Sariciftci, P. Stadler, *Adv. Mater. Interfaces* **2020**, *7*, 1901364.
[49] D. Farka, H. Coskun, J. Gasiorowski, C. Cobet, K. Hingerl, L. M. Uiberlacker, S. Hild, T. Greunz, D. Stifter, N. S. Sariciftci, R. Menon, W. Schoefberger, C. C. Mardare, A. W. Hassel, C. Schwarzinger, M. C. Scharber, P. Stadler, *Adv. Electron. Mater.* **2017**, 1700050.
[50] P. Stadler, *Synth. Met.* **2019**, *254*, 106.
[51] S. Kivelson, A. Heeger, *Synth. Met.* **1988**, *22*, 371.